MOLECULAR HYDROGEN DEFICIENCY IN H I-POOR GALAXIES AND ITS IMPLICATIONS FOR STAR FORMATION

Michele Fumagalli[1], Mark R. Krumholz[1], J. Xavier Prochaska[1,2], Giuseppe Gavazzi[3], and Alessandro Boselli[4]

[1] Department of Astronomy and Astrophysics, University of California, 1156 High Street, Santa Cruz, CA 95064, USA; mfumagalli@ucolick.org
[2] UCO/Lick Observatory; University of California, 1156 High Street, Santa Cruz, CA 95064, USA
[3] Dipartimento di Fisica G. Occhialini, Universita' di Milano—Bicocca, Piazza della scienza 3, Milano, Italy
[4] Laboratoire d'Astrophysique de Marseille, UMR 6110 CNRS, 38 rue F. Joliot-Curie, F-13388, Marseille, France

ABSTRACT

We use a sample of 47 homogeneous and high-sensitivity CO images taken from the Nobeyama and BIMA surveys to demonstrate that, contrary to common belief, a significant number ($\sim$ 40%) of H I-deficient nearby spiral galaxies are also depleted in molecular hydrogen. While H I deficiency by itself is not a sufficient condition for molecular gas depletion, we find that H_2 reduction is associated with the removal of H I inside the galaxy optical disk. Those H I-deficient galaxies with normal H_2 content have lost H I mainly from outside their optical disks, where the H_2 content is low in all galaxies. This finding is consistent with theoretical models in which the molecular fraction in a galaxy is determined primarily by its gas column density. Our result is supported by indirect evidence that molecular deficient galaxies form stars at a lower rate or have dimmer far infrared fluxes than gas rich galaxies, as expected if the star formation rate is determined by the molecular hydrogen content. Our result is consistent with a scenario in which, when the atomic gas column density is lowered inside the optical disk below the critical value required to form molecular hydrogen and stars, spirals become quiescent and passive evolving systems. We speculate that this process would act on the timescale set by the gas depletion rate and might be a first step for the transition between the blue and red sequence observed in the color–magnitude diagram.

Key words: galaxies: evolution – galaxies: ISM – galaxies: spiral – ISM: molecules – stars: formation

Online-only material: color figures

1. INTRODUCTION

A complete and coherent description of the detailed connection between a galaxy's gaseous phase and its star formation is still lacking. This poses a significant limitation for studying galaxy evolution, even in the local universe. From an observational point of view, two different approaches have been adopted to address this fundamental topic. The first takes advantage of high spatial resolution images to compare directly the molecular and atomic phases of the interstellar medium (ISM) with recent star formation activities. The results (Wong & Blitz 2002; Kennicutt et al. 2007; Fumagalli & Gavazzi 2008; Bigiel et al. 2008) suggest that stars form preferentially in molecular regions, as traced by diffuse CO emission. The second approach is more indirect, but relies on estimators for the star formation rate (SFR) and atomic gas that can be easily collected for large samples. These projects statistically study the effects of the atomic gas removal on star formation in cluster galaxies compared with field galaxies. Results (Kennicutt & Kent 1983; Gavazzi et al. 2002; Koopmann & Kenney 2004; Gallazzi et al. 2009; G. Gavazzi et al. 2009, in preparation) show a significant correlation between the atomic gas and the star formation: the latter is quenched in those galaxies which are H I deficient due to environmental effects. Although this result can be interpreted in terms of H I feeding star formation (Boselli et al. 2001), it is possible that molecular hydrogen (H_2) depletion also plays a critical role.

However, observations to date suggest that molecular hydrogen, which dominates the mass of the interstellar medium in the center of spiral galaxies, is not strongly affected by environmental perturbations. Galaxies in rich clusters appear to have on average the same molecular content as field galaxies (Stark et al. 1986; Kenney & Young 1986, 1989; Casoli et al. 1991; Boselli et al. 1997, 2002). This result is consistent with a simple theoretical argument based on the assumption that ram-pressure stripping is the dominant environmental process, a fact that, although not yet proved, is likely to be the correct interpretation for H I observations in the Virgo and Coma clusters (see a review by Boselli & Gavazzi 2006). According to this picture, a galaxy which travels at a velocity v_{rel} relative to the dense intergalactic medium (IGM) or intracluster medium (ICM) characterized by a density ρ_{IGM} looses its ISM at the escape velocity v_{esc} and density ρ_{ISM} only if

$$\rho_{IGM} v_{rel}^2 > \rho_{ISM} v_{esc}^2 . \tag{1}$$

This condition is not easily satisfied for gas in molecular hydrogen phase, which has densities up to 10^5 cm^{-3}, and is usually strongly bound to the galaxy due to its proximity to the galactic center.

This theoretical argument seems to agree with observations of the CO abundance in members of the Virgo and Coma clusters. Using a sample composed of 47 Virgo galaxies, Stark et al. (1986) showed that the molecular fraction CO/H I increases toward the center of the cluster, identified by the position of M87. This is consistent with the removal of atomic hydrogen only from inner cluster galaxies, without any corresponding change in the molecular hydrogen content. With independent CO measurements, the same conclusion was reached by Kenney & Young (1986, 1989), who studied molecular hydrogen deficiency in data sets of 23 and 41 Virgo galaxies. Their analysis shows that the molecular content has not responded to the H I removal on timescales of 10^9 yr, i.e., it is unperturbed within the Virgo crossing time. Furthermore, Casoli et al. (1991) pointed out that even in the Coma cluster, where the

ram-pressure is stronger than in Virgo, there is no correlation between the H$_2$ mass and the atomic hydrogen content of individual spirals. Surprisingly, using the data collected by Kenney & Young (1989) with updated distances, Rengarajan & Iyengar (1992) found from a comparison of normalized H$_2$ masses that some deficiency of molecular hydrogen holds among Virgo galaxies, as compared to the field. This result is in contrast with a series of papers by Boselli et al. (1997, 2002), who did not find any correlation between the H I and the H$_2$ deficiency on a large sample of $\sim$ 250 Virgo and Coma galaxies. Except some extreme cases of galaxies which have their molecular gas depleted and displaced (e.g., Vollmer et al. 2008), there is no strong evidence that cluster member galaxies have statistically less molecular gas than field galaxies.

This seems in contradiction with a coherent picture of the star formation in spirals. If stars really do form primarily in molecular gas, one might expect the quenching in the star formation activity to be connected with a molecular gas deficiency in H I-poor galaxies. This hypothesis is partially supported by Fumagalli & Gavazzi (2008), who, using a small sample of 28 images from the Nobeyama CO survey (Kuno et al. 2007), find some hints of a possible depletion in the molecular content (see their Figure 4 and 6). The aim of this paper is a test for H$_2$ deficiency by using homogeneous and high-sensitivity data from the Nobeyama (Kuno et al. 2007), BIMA (Helfer et al. 2003), VIVA (A. Chung et al. 2009, in preparation) and THINGS (Walter et al. 2008) surveys. At first, we compare the integrated molecular and atomic gas mass; then, we study the distribution of the gas as a function of the galaxy radius and finally we compare both the atomic and hydrogen gas content with indicators for the star formation. While previous studies selected galaxies mainly from the Virgo and Coma clusters, our sample includes also objects from nearby groups. In these diverse environments it is less obvious that ram-pressure is the most efficient process in removing the atomic gas. Therefore, in our analysis we will focus only on the effects produced by the H I removal, without addressing to the details of its origin that is likely connected with a generic environmental perturbations or galaxy feedback.

The paper is organized as follows: the sample and the data reduction are discussed in Section 2, the analysis is given in Section 3 and the discussion in Section 4. In particular, we focus on why previous surveys did not detect the H$_2$ deficiency (Section 4.1), we explain the process responsible for the molecular gas depletion (Section 4.2) and we discuss the implications of H$_2$ deficiency on the star formation (Section 4.3). The conclusions are in Section 5.

2. DATA REDUCTION

2.1. The Sample

Our sample is selected based on the criterion of high-sensitivity CO images and homogeneity to minimize the scatter in CO measurements. Because previous CO surveys show a relative flux dispersion which severely limits the H$_2$ deficiency analysis (see Section 4.1), we limit to the Nobeyama CO survey (Kuno et al. 2007) and the BIMA survey (Helfer et al. 2003) which are shown to agree to within 0.4 dex. Forty-seven massive spiral galaxies in the H-band luminosity range $10^{10} \leqslant L_H/L_\odot \leqslant 10^{11}$ meet our selection criterion, 40 from the Nobeyama survey and seven from BIMA. Our sample includes only spiral galaxies since early-type (E/dE) galaxies are known to be extremely gas poor (di Serego Alighieri et al. 2007), while

late-type galaxies (Sa–Sc, BCD or Irr/dIrr) are typically gas rich (Gavazzi et al. 2008). Table 1 summarizes some observational properties for our sample. Since we are dealing mainly with the full Nobeyama CO atlas, which has been selected using a far infrared (FIR) emission criterion ($F_{100\,\mu m} > 10$ Jy), our sample may be biased against CO-poor galaxies.

The Nobeyama maps are obtained with a 45 m single-dish radio telescope that provides high-sensitivity ($\sim$ 0.5 $M_\odot$ pc^2) flux measurements for the entire galaxy disk. The spatial resolution is about 15$''$, which corresponds to an average physical scale of $\sim$ 1 kpc at the mean distance of our sample ($\sim$ 15 Mpc). In contrast, despite its higher spatial resolution (6$''$–10$''$, corresponding to 450–700 pc), the interferometric BIMA survey has systematically poorer sensitivity to extended flux because interferometers cannot detect flux from regions larger than the size-scale set by the minimum distance between the antennas. One can recover the total flux by using single dish observations that provide the zero spacing element. We have limited our galaxy sample to the subset with single-dish data. Even for these galaxies, the reconstruction algorithm is biased against large scales (Helfer et al. 2003, Appendix A); however, a comparison between Nobeyama and BIMA data indicates that the missed flux is negligible compared to the total flux, i.e., the BIMA survey provides a reliable estimate of the integrated molecular hydrogen mass. When a galaxy is imaged in both the surveys, we use the Nobeyama data.

For our analysis we will also compare the spatial distributions of molecular and atomic hydrogen; therefore we collect spatially resolved H I images from the THINGS survey (Walter et al. 2008) and the VIVA survey (A. Chung et al. 2009, in preparation). Since spatially resolved images are not available for all the galaxies in our sample, while studying surface density profiles we restrict our analysis to a subsample of 20 galaxies (see Table 1).

2.2. A Multifrequency Analysis

Comparison between the molecular distribution, the atomic hydrogen content, and the star formation activity requires some preliminary transformations from observed to physical quantities. In this section we describe this issue.

2.2.1. The Molecular Hydrogen

The H$_2$ molecule has no permanent dipole so we must infer its abundance indirectly by assuming that the conditions of the ISM where the H$_2$ forms are similar to those in which other molecules are synthesized. A good tracer for H$_2$ is CO because the intensities of its rotational transitions are correlated to the molecular column density. This is based on a simple argument which relates the velocity inferred from the line profile with the virial velocity of molecular clouds (Dickman et al. 1986; Solomon et al. 1987).

The Nobeyama and BIMA surveys image the CO J : 1–0 transition at 115 GHz, which is excited above 5.5 K in cool gas at moderate density. We infer the molecular hydrogen column density by adopting a conversion factor X (cm^{-2} (K km s^{-1})$^{-1}$), which is a function of temperature, density, UV radiation field, metallicity and even of the shape of the molecular clouds (Wall 2007; Boselli et al. 2002, 1997, Appendix A). Because it is impossible to model X theoretically for actual galaxies, a constant conversion factor derived using observations in our Galaxy has often been assumed (e.g., Solomon et al. 1987). The Galactic factor likely gives underestimates for the molecular hydrogen content in low-mass galaxies, because empirical

Table 1
Properties of Our Galaxy Sample

Name	R.A. (deg)	Decl. (deg)	Dist. (Mpc)	Type	L_H ($L_\odot$)	R_{25} (")	def$_{H_2}$	def$_{H_1}$	Hα+ [N II] (EW Å)	CO Ref.[a]
IC 342	56.70	68.10	3.9	Sc	10.5	598	−0.24	−0.78	56	N
Maffei 2	40.48	59.60	3.4	Sbc	10.1	174	−0.10	−0.17	...	N
NGC 0253	11.89	−25.29	3.0	Sc	10.6	789	0.10	0.65	16	N
NGC 0628	24.17	15.78	9.7	Sc	10.5	293	0.19	−0.01	35	B*
NGC 1068	40.67	−0.01	14.4	Sb	11.1	184	−0.11	0.47	50	N
NGC 2903	143.04	21.50	6.3	Sb	10.4	352	0.02	0.33	18	N*
NGC 3184	154.57	41.42	8.7	Sc	10.2	222	0.11	0.32	...	N*
NGC 3351	160.99	11.70	8.1	Sb	10.4	217	0.34	0.60	16	N*
NGC 3504	165.80	27.97	26.5	Sab	10.7	73	0.10	0.37	35	N
NGC 3521	166.45	−0.03	7.2	Sb	10.6	249	0.19	0.06	20	N*
NGC 3627	170.06	12.99	6.6	Sb	10.5	306	−0.11	0.81	19	N*
NGC 3631	170.26	53.17	21.6	Sc	10.7	111	0.01	−0.03	34	N
NGC 3938	178.20	44.12	17.0	Sc	10.5	106	−0.06	−0.24	26	B
NGC 4051	180.79	44.53	17.0	Sb	10.6	146	−0.03	0.26	32	N
NGC 4102	181.60	52.71	17.0	Sb	10.5	88	−0.02	0.47	26	N
NGC 4192	183.45	14.90	17.0	Sb	11.0	293	0.59	0.36	9	N
NGC 4212	183.91	13.90	16.8	Sc	10.3	108	0.17	0.57	20	N
NGC 4254	184.71	14.42	17.0	Sc	10.9	184	−0.20	0.18	32	N
NGC 4258	184.74	47.30	6.8	Sb	10.7	545	0.44	0.25	15	B
NGC 4303	185.48	4.47	17.0	Sc	11.0	197	−0.08	0.13	36	N
NGC 4321	185.73	15.82	17.0	Sc	11.1	273	0.05	0.53	18	N*
NGC 4402	186.53	13.11	17.0	Sc	10.4	118	0.02	0.73	12	N
NGC 4414	186.61	31.22	17.0	Sc	10.9	108	−0.09	−0.15	23	N
NGC 4419	186.74	15.05	17.0	Sa	10.6	105	0.40	1.04	7	N*
NGC 4501	188.00	14.42	17.0	Sbc	11.2	216	0.14	0.51	6	N
NGC 4535	188.58	8.20	17.0	Sc	10.8	249	0.02	0.35	17	N
NGC 4536	188.61	2.19	17.0	Sc	10.7	216	0.18	0.29	20	N*
NGC 4548	188.86	14.50	17.0	Sb	10.9	180	0.84	0.70	17	N
NGC 4569	189.21	13.16	17.0	Sab	11.0	321	0.23	1.13	2	N*
NGC 4579	189.43	11.82	17.0	Sab	11.1	188	0.62	0.71	4	N
NGC 4654	190.99	13.13	17.0	Sc	10.7	149	−0.02	0.17	31	N*
NGC 4689	191.94	13.76	17.0	Sc	10.5	175	0.14	1.06	14	N*
NGC 4736	192.72	41.12	4.3	Sab	10.4	232	0.78	0.68	10	N*
NGC 4826	194.18	21.68	4.1	Sab	10.3	314	0.70	0.86	9	B*
NGC 5005	197.73	37.06	21.3	Sb	11.3	143	0.28	0.47	7	B
NGC 5033	198.36	36.59	18.7	Sc	11.0	293	−0.16	0.19	20	B
NGC 5055	198.96	42.03	7.2	Sbc	10.7	352	0.04	0.12	20	N*
NGC 5194	202.47	47.19	7.7	Sbc	10.8	232	−0.36	0.12	28	N*
NGC 5236	204.25	−29.86	4.7	Sc	10.7	464	0.23	−0.49	33	N*
NGC 5247	204.51	−17.88	22.2	Sb	10.9	161	0.06	0.05	...	N
NGC 5248	204.38	8.88	22.7	Sb	11.1	122	−0.10	−0.25	26	N
NGC 5457	210.80	54.35	5.4	Sc	10.5	719	0.06	0.28	31	N*
NGC 6217	248.16	78.20	23.9	Sbc	10.5	67	0.13	−0.45	34	N
NGC 6946	308.72	60.15	5.5	Sc	10.4	344	−0.28	−0.45	34	N*
NGC 6951	309.31	66.10	20.3	Sb	11.1	97	0.24	0.04	16	N
NGC 7331	339.27	34.42	14.3	Sbc	11.1	273	0.14	−0.04	...	B*
UGC 2855	57.09	70.13	20.3	Sc	10.9	132	−0.34	−0.13	34	N

Notes.
[a] N: Nobeyama survey (Kuno et al. 2007); B: BIMA survey (Helfer et al. 2003). Galaxies included in the high-resolution study are identified by an asterisk.
References. References are discussed throughout the text.

calibrations show that X decreases for increasing mass (e.g., Boselli et al. 2002). Since we expect the CO-to-H$_2$ conversion factor to depend primarily on the dust and metallicity that regulate the formation and photodissociation of H$_2$ and the CO heating, we choose an individual X value for each galaxy following the empirical calibrations of Boselli et al. (2002). This is

$$\log X = -0.38 \log L_H + 24.23 , \qquad (2)$$

where L_H is the H-band luminosity in $L_\odot$. We retrieve L_H from GOLDMine (Gavazzi et al. 2003) and SIMBAD. This calibra-

tion accounts for the dependence of X on the metal abundance because the H-band luminosity correlates with galaxy metallicity (e.g., Boselli et al. 2002). The systematic uncertainty on the X factor derived using Equation (2) ranges from 0.65 to 0.70 dex for the luminosity interval 10^{10}–10^{11} $L_\odot$. Other unknown dependencies can increase this error. The final conversion for the molecular hydrogen surface density is

$$\Sigma_{H_2} [M_\odot \text{ cm}^{-2}] = 2m_p X F_{co} , \qquad (3)$$

where m_p is the proton mass in $M_\odot$ and F_{co} is the CO flux in

K km s^{-1}. This conversion does not include the mass of helium, but its contribution may be included trivially by multiplying the derived surface density by 1.36. The integrated CO flux (F_{co} in Jy km s^{-1}) is converted into a total H$_2$ mass (M_{H_2} in $M_\odot$) using (Helfer et al. 2003)

$$M_{H_2} = 3.92 \times 10^{-17} X \bar{F}_{co} D^2 , \qquad (4)$$

where D is the galaxy distance in Mpc from GOLDMine and Tully (1994).

2.2.2. The Atomic Hydrogen

We estimate the atomic hydrogen content via the 21 cm emission line. Single-dish H I surveys, including the ALFALFA (Giovanelli et al. 2005) or HIPASS (Meyer et al. 2004) surveys, do provide the H I integrated flux for all the galaxies in our sample. Collecting different H I data for a same galaxy, we notice a significant dispersion in the measured H I flux, even up to a factor of 2. Because we are interested in a relative comparison between galaxies rather than an accurate determination of the absolute H I mass, we retrieve all the H I fluxes from the HyperLeda database (Paturel et al. 2003a). Even if more recent measurements have better sensitivity and provide a more accurate determination of the total H I abundance, this approach gives a homogeneous data set (Paturel et al. 2003b). As discussed in the Appendix, a particular choice for the observed flux does not affect our analysis.

The integrated H I flux ($\bar{F}_{H I}$ in Jy km s^{-1}) is converted into a total mass ($M_{H I}$ in $M_\odot$) using

$$M_{H I} = 2.36 \times 10^5 \bar{F}_{H I} D^2 , \qquad (5)$$

where D is the galaxy distance in Mpc from GOLDMine and Tully (1994). The H I surface density profile is computed from THINGS and VIVA images according to the conversion

$$\Sigma_{H I} [M_\odot \, cm^{-2}] = m_p N_{H I} , \qquad (6)$$

where $N_{H I}$ is the column density in cm^{-2} derived from the flux $F_{H I}$ (Jy beam^{-1} km s^{-1}) using the following calibration (e.g., Walter et al. 2008),

$$N_{H I}[10^{19} cm^2] = 110.4 \times 10^3 \frac{F_{H I}}{B_{min} \times B_{max}}, \qquad (7)$$

with B being the beam FWHM in arcsec. As with H$_2$, these surface densities do not include the mass of helium.

2.2.3. The Star Formation Activity

In the ISM of galaxies, the Hα emission line is caused by the recombination of atomic hydrogen which has been ionized by the UV radiation of O and B stars. Therefore Hα is a tracer of recent, massive ($M > 10 \, M_\odot$) star formation activity on timescales of $t \leqslant 4 \times 10^6$ yr (Kennicutt 1998). For all but three objects, we retrieve from the literature (GOLDmine; Kennicutt & Kent 1983; James et al. 2004; Kennicutt et al. 2008) the Hα equivalent width (EW), a tracer of the SFR (Kennicutt 1983b).

Since the narrow band filter used to image the Hα emission line is large enough to collect the flux from the [N II] line, the measured EW overestimates the Hα emission. Unfortunately, the ratio [N II]/Hα is not available for all of the galaxies in our sample and we can apply only the average correction [N II]/Hα = 0.53, as suggested by Kennicutt (1992). However, this value underestimates the [N II] emission from the bulges of

galaxies that host active galactic nuclei (AGNs), where the nuclear [N II] can be even stronger than the Hα. In addition, even if the nuclear emission were corrected using a suitable factor, it would not be possible to disentangle between the Hα flux due to star formation from that due to AGN ionization. Our sample, composed of massive spirals, is likely to be affected by this contamination (Decarli et al. 2007).

Another effect to consider is dust absorption. In principle, one can estimate the extinction by measuring the Hα/Hβ or the Hα/Br$_\gamma$ fluxes (case B recombination). These values, however, are unknown for the majority of our galaxies. One could apply a standard dust extinction (e.g., $A = 1.1$ mag; Kennicutt & Kent 1983) but this would not change the relative distribution of the measurements. Instead, we simply keep the measured Hα+ [N II] EW as an approximation for the specific SFR. The reader should keep in mind that a large uncertainty is associated with these measurements, in addition to the error in the flux determination.

2.3. Global Fluxes and Surface Brightness Profiles

We compute total CO fluxes from the Nobeyama images using the IRAF task qphot by integrating the emission in an aperture which encloses the entire galaxy. Fluxes from the BIMA survey are retrieved from Helfer et al. (2003), who list values computed within a square region. We retrieve the H I flux from HyperLeda, as previously discussed. We compute the surface brightness profiles for the CO and H I using an IDL procedure that averages the flux into elliptical annuli characterized by three fixed parameters (the galaxy center, the eccentricity, and the position angle); we adopt a step along the major axis of $\sim$ 5 arcsec, roughly 1/3 of the spatial resolution of the CO images from the Nobeyama survey. All the profiles are corrected for the projection effect using the galaxy inclination (HyperLeda) on the plane of the sky. For each galaxy we finally obtain the H I and H$_2$ surface density profiles $\Sigma_{H I}$ and Σ_{H_2} in $M_\odot$ pc^{-2}.

3. ANALYSIS

To test for molecular hydrogen depletion in our data set, we compare the H$_2$ mass in a sample of isolated galaxies with that in perturbed galaxies. Our isolation criterion is defined by the atomic hydrogen content. Because the edges of the H I disk are weakly bounded, any perturbation can easily remove atomic gas from a galaxy, lowering its H I mass. That the H I deficiency should trace environmental effects is supported by Giovanelli & Haynes (1985), who show that H I deficiency increases toward the center of a cluster. In these regions the IGM is dense, the cluster potential well is deep and the number of galaxies is high so that environmental processes are very effective. We expect H I deficiency to be a useful measure of disturbance even if environment is not the dominant means of gas removal. For example, if star formation feedback is the primary cause of gas loss, this too will preferentially remove the low–density, loosely bound H I.

Formally, the atomic gas depletion is quantified using def$_{H I}$, the deficiency parameter, defined by Haynes & Giovanelli (1984) as the logarithmic difference between the expected H I mass in isolated galaxies and the observed value:

$$def_{H I} = \log M_{H I,exp} - \log M_{H I,obs}. \qquad (8)$$

The reference mass $M_{H I,exp}$ is computed as a function of the optical radius at the 25th mag arcsec^{-2} in the B band (retrieved
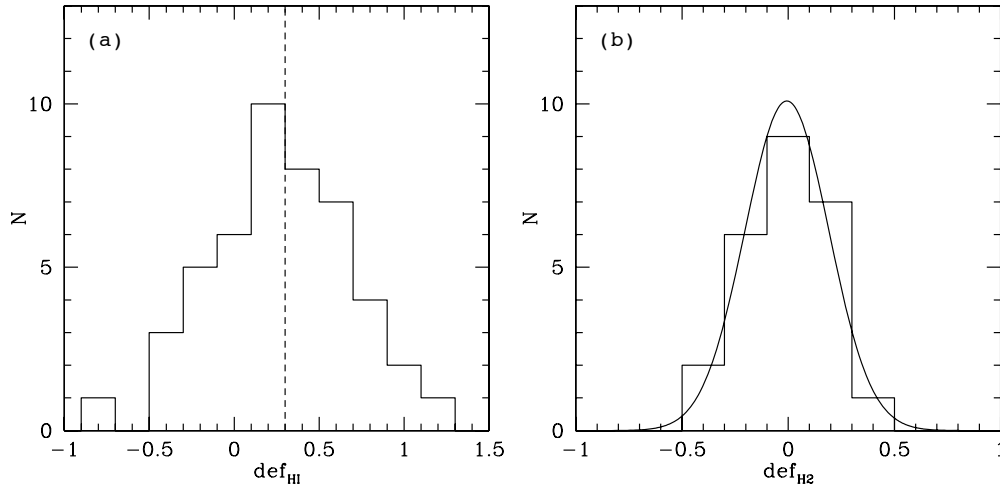
Figure 1. (a) Histogram of the H I-deficiency values in our sample, separated in isolated and perturbed galaxies at $def_{H I} = 0.3$. A positive value of $def_{H I}$ indicates that a galaxy has an H I mass lower than expected on average according to its size and morphology. (b) Histogram of the H$_2$-deficiency values for isolated galaxies only. The Gaussian fit shows that $\sigma = 0.2$.

from NED and HyperLeda) using the coefficients recently updated by Solanes et al. (1996), which are weakly dependent on the morphological type. Several sources of uncertainty affect the determination of $def_{H I}$: the error on the observed H I mass, the statistical uncertainty on the calibrated coefficients and the determination of the optical diameter. It is hard to quantify a value for the final uncertainty, but a comparison of the values derived for a single galaxy using different data available in the literature suggests a mean dispersion of 0.2–0.3 dex on the H I deficiency.

Figure 1(a) shows the distribution of the H I deficiencies for our sample. If we arbitrarily consider unperturbed those galaxies which have lost less than a factor of 2 in their H I mass ($def_{H I} < 0.3$), our subsample of isolated galaxies is composed of 25 objects with a mean deficiency $def_{H I} = -0.045 \pm 0.27$. This is consistent with zero. Moreover, we point out that the dispersion on the mean value is within the deficiency threshold of 0.3 dex. Only 4 galaxies lie at $def_{H I} < -0.3$, indicating that our reference sample is not dominated by galaxies with H I mass above the average. The remaining 22 galaxies have $def_{H I} \geqslant 0.3$, spanning the entire range of moderate and high deficiencies (0.3–1.2 dex).

In a similar way, we quantify a possible reduction in the molecular hydrogen content using the H$_2$-deficiency parameter def_{H_2} (Boselli et al. 1997, 2002):

$$def_{H_2} = \log M_{H_2,exp} - \log M_{H_2,obs} . \qquad (9)$$

The value for the reference mass $M_{H_2,exp}$ is computed from the observed correlation between the H$_2$ and the H-band luminosity (Boselli et al. 1997) for isolated galaxies ($def_{H I} < 0.3$). This definition is based on the natural scaling of the molecular gas abundance with the size of a galaxy, i.e., more massive spiral galaxies are more gas rich. Although our sample covers a small range in luminosity, owing to the good quality of our data (see Section 4.1), we choose to compute a new reference mass with a least-squares fit:

$$\log M_{H_2,exp} = 0.50 \log L_H + 3.98 . \qquad (10)$$

Since the dispersion (rms) in the calibration is ~ 0.2 (see also Figure 1(b)), galaxies with $def_{H_2} < 0.2$ cannot be distinguished from normal galaxies. In the following analysis we therefore

consider a galaxy H$_2$-deficient only if $def_{H_2} \geqslant 0.2$. However, as we shall see below, def_{H_2} shows a continuous rather than a bimodal distribution. Thus, this criterion is arbitrary. It does have the virtue, though, of nicely dividing our sample into classes which have a comparable number of objects. As with $def_{H I}$, it is hard to quantify an uncertainty for def_{H_2}. Deficiency is a relative quantity, so the level of uncertainty for def_{H_2} is likely to be significantly lower than for the absolute H$_2$ mass. The error of 0.7 dex we quoted in Equation (2) is therefore an upper limit on the scatter in def_{H_2}. A more reliable estimate of the error is the dispersion of 0.2 dex we measure in def_{H_2} for the control sample of isolated galaxies (Figure 1(b)). Since random error in computing M_{H_2}, for example galaxy-to-galaxy scatter in X, can only broaden the intrinsic dispersion of H$_2$ masses at fixed L_H, our measured scatter of 0.2 dex sets a more realistic upper limit on the size of random errors. The one caveat is that this value may neglect systematic uncertainties if unperturbed and perturbed galaxies have different values of luminosity or metallicity, for example, and thus systematically different values of X. However, we do not observe or expect any obvious trend of these quantities as a function of $def_{H I}$ or def_{H_2}.

Figure 2 shows a comparison between def_{H_2} and $def_{H I}$ in our sample. The vertical dashed line corresponds to $def_{H I} = 0.3$ dex, the value below which a galaxy is considered unperturbed; the horizontal line represents $def_{H_2} = 0.2$ dex. Inspecting this plot, the first striking result is that 9/22 of the galaxies with $def_{H I} \geqslant 0.3$ have def_{H_2} values greater than 0.2 dex, while the region characterized by $def_{H I} < 0.3$ and $def_{H_2} \geqslant 0.2$ is almost empty. This distribution proves the existence of the molecular deficiency in a significant number of galaxies which are H I poor. This figure indicates that def_{H_2} and $def_{H I}$ do not follow a tight correlation, but this is not surprising. In fact, we do not expect effects that deplete the H I to act in the same way on the H$_2$ gas which is more strongly bound. Rather than a correlation, it is evident that galaxies lie in three regions roughly defined by our criterion of isolation and molecular deficiency (dashed lines). Based on Figure 2, we divide our sample into three classes: *unperturbed* or *nondeficient* galaxies ($def_{H I} < 0.3$ and $def_{H_2} < 0.2$), *gas-deficient* galaxies ($def_{H I} \geqslant 0.3$ and $def_{H_2} \geqslant 0.2$) and galaxies which are only H I-*deficient* ($def_{H I} \geqslant 0.3$ and $def_{H_2} < 0.2$). This classification should not be considered strict, since galaxies are distributed continuously rather than in
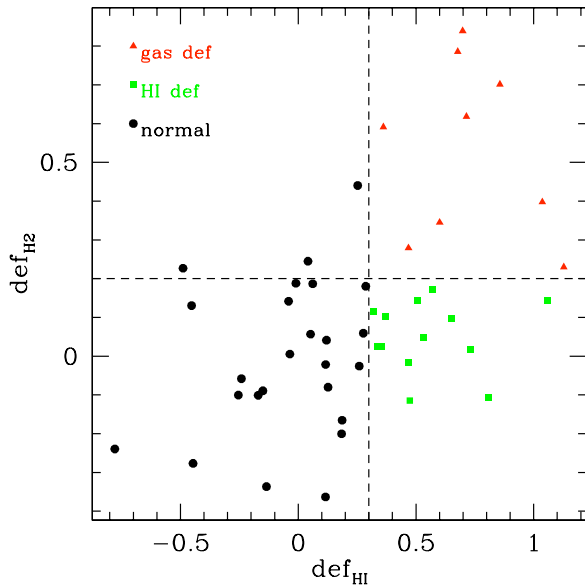
Figure 2. Comparison between calculated def_{H_2} and def_{H_I} values for our sample. The vertical dashed line corresponds to $def_{H_I} = 0.3$ dex, the value below which a galaxy is considered unperturbed; the horizontal line represents $def_{H_2} = 0.2$ dex. The absence of galaxies in the upper left quadrant suggests that H I deficiency is only a necessary condition for H_2 deficiency.

(A color version of this figure is available in the online journal.)

distinct populations, but it is useful for the analysis. We test the robustness of our result by changing the isolation criterion in the range $def_{H_I} = 0.1–0.4$ and recomputing def_{H_2} after that a new calibration has been derived. We find that the distribution in Figure 2 does not change significantly.

Since the definition of the molecular gas deficiency relies on Equation (10) which sets the reference mass, the behavior shown in Figure 2 could be an artifact imposed by this calibration. We further explore the robustness of a H_2-deficient population by studying the H_2 deficiency with surface density gas profiles, which is independent from the calibration of $\log M_{H_2,\exp}$. In Figure 3 we show the average molecular gas surface density profiles, in bins of normalized galactocentric radius[5] (R/R_{25}). Not all the galaxies in our sample are imaged in H I. Therefore, for this kind of analysis, we consider only 20 galaxies (see Table 1). Details on the completeness in each class are provided in Table 2. By comparing the values for the three classes of galaxies (nondeficient with circles, gas-deficient with triangles, and H I-deficient with squares), it is evident that gas-deficient galaxies have the lowest molecular gas column densities, while H I-deficient and nondeficient galaxies exhibit a similar behavior. The dashed line in Figure 3 shows the average profile excluding those galaxies with $def_{H_I} < -0.3$. The similarity of this profile to that of the full nondeficient sample (circles) indicates that the observed difference in H_2 content between the three galaxy classes is not an artifact enhanced by the presence of gas-rich galaxies in our sample. Based on an independent method, Figure 3 confirms the existence of H_2-deficient galaxies in ∼ 40% of the H I-poor galaxies and ∼ 20% of all the galaxies in our sample. As discussed in the next section, these values should be regarded as lower limits.

---

[5]   This quantity is well defined under the hypothesis that the stellar disk is not truncated during the perturbation. Clearly this is not the case for tidal interactions. In our sample, NGC 3351 is the galaxy most likely to be affected by tidal stripping. However, we note that a value for R_{25} larger than what we have adopted would shift the surface density profile at lower R/R_{25}, enhancing the separation between unperturbed and gas-deficient galaxies.
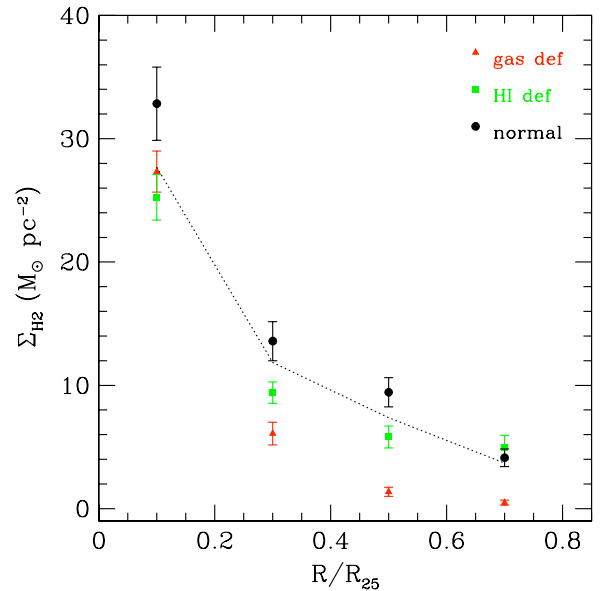
Figure 3. Average H_2 profiles in bins of normalized radius. The dashed line is computed by excluding H I-rich galaxies with $def_{H_I} < -0.3$. The offset among the profiles reflects the def_{H_2} distribution in Figure 2.

(A color version of this figure is available in the online journal.)

Table 2
Completeness for the Surface Density Profiles

Class	Objects	% Class[a]	% Total[b]	Symbol[c]
Nondeficient	10	40%	21%	Circle
Non-gas-rich	8	38%	17%	Line
H I-deficient	5	38%	11%	Square
Gas-deficient	5	56%	11%	Triangle

Notes.
[a] % Class is defined as the number of galaxies with H I maps in each class over the total number of objects in that class.
[b] % Total is defined as the number of galaxies with H I maps in each class over 47, the number of objects in the entire sample.
[c] Symbols used for each class in the plots throughout the paper.

4. DISCUSSION

4.1. Comparison with Previous Studies

The first issue that we would like to address is why previous studies, based on large CO surveys, did not reveal a population of H_2-deficient galaxies. As discussed in the introduction, several studies (Stark et al. 1986; Kenney & Young 1986, 1989; Casoli et al. 1991; Boselli et al. 1997, 2002) based on large samples both in the Virgo and in the Coma clusters did not show any evidence for a molecular gas deficiency. As discussed by Boselli & Gavazzi (2006), some biases influence the previous works; for example, a constant X conversion factor was often assumed or samples were selected according to FIR selection criteria which prefer CO rich galaxies. Of course, our sample has also been selected to have IRAS fluxes from the Point Source Catalogue higher than 10 Jy at 100 μm. By comparing the 100 μm flux with our def_{H_2} in Figure 4, we notice that gas-deficient galaxies show systematically lower 100 μm luminosity; therefore, we might miss a significant fraction of molecular poor galaxies.

Based on this work, we can identify two additional reasons for why previous studies failed to detect the molecular deficiency: the completeness in the flux sampling and the homogeneity of the data. While observing at a single dish, the integration time
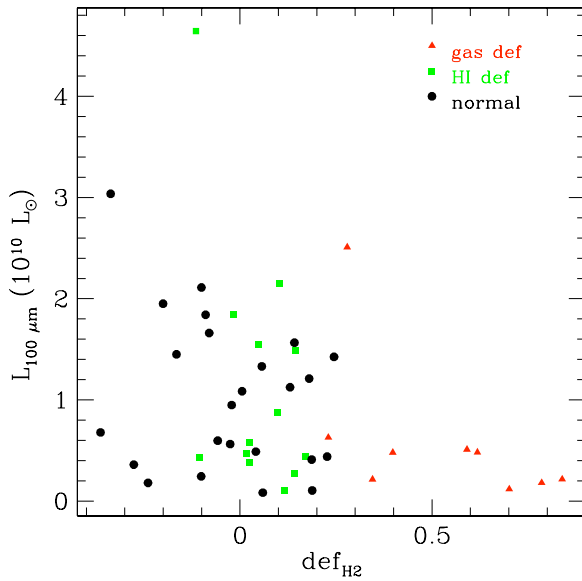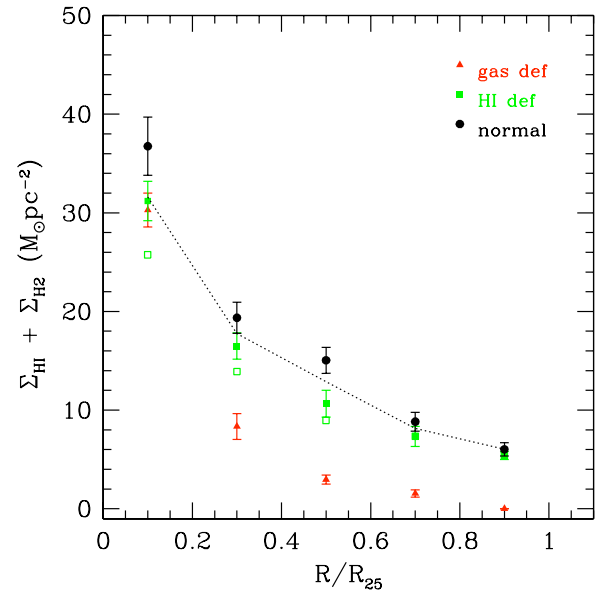
Figure 4. Far infrared luminosity at 100 μm as a function of the molecular gas deficiency. Gas-deficient galaxies show the lowest 100 μm luminosity.

(A color version of this figure is available in the online journal.)

Figure 5. Average total gas surface density profiles in bins of normalized radius, divided according to their $def_{H\,I}$ and def_{H_2} values. The dashed line is computed excluding H I rich galaxies with $def_{H\,I} < -0.3$ and the open squares indicate the profile for H I-deficient galaxies without NGC 4321. Gas-deficient galaxies have in the disk a gas column density below the values required to form molecular hydrogen ($\sim 10\ M_\odot\ pc^{-2}$).

(A color version of this figure is available in the online journal.)

required to detect the CO flux is very high (120 minutes at a 12 m telescope are needed to reach a sensitivity of 3 mK at a resolution of 15 km s^{-1}) and several observations are required to image the entire galaxies. It has only recently become possible produce CO images in a reasonable observing time, thanks to the availability of multibeam receivers that reduce the number of pointings required to fully map the entire disk. Due to these technical limitations, previous studies were based on the observation of one position per galaxy plus one or two positions off-center, along the major axis. The total CO flux was then recovered by interpolating with an exponential profile, a procedure that inevitably gives only a rough estimate of the proper H$_2$ mass. By comparing the integrated CO flux from Kenney & Young (1988) and GOLDMine with the Nobeyama and BIMA data, we find a dispersion of up to 1 dex. In contrast, by comparing galaxies in common in the BIMA and Nobayama surveys, the observed discrepancy in the total mass is less than 0.4 dex. Therefore, we believe that the data used in previous studies suffer from fluctuations larger than the observable H$_2$ deficiency (< 0.8 dex in our sample). Another possible problem is related to the homogeneity of the sample. To increase the statistics, earlier studies often combined CO data from surveys with different sensitivities and diverse techniques to recover the integrated flux, increasing the relative dispersion in the observed H$_2$ mass. We attribute the fact that the H$_2$ deficiency has remained hidden in previous analysis to the combination of these two effects. In contrast, based on high quality and homogeneous data from the BIMA and Nobeyama surveys, our work allows for a determination of molecular gas deficiency.

4.2. The Observed Distribution in the H$_2$ Deficiency

The observed distribution in def_{H_2} deserves a detailed analysis. In particular, we are interested in understanding why H I deficiency is a necessary but insufficient condition for H$_2$ deficiency and what the fundamental difference is between galaxies which are only H I-deficient and galaxies which are also molecular gas deficient. The answers to these questions lie in the physics that governs the H$_2$ formation. Molecular hydrogen is synthesized in spiral disks through the interaction of atomic hydrogen

with dust grains, whereas it is destroyed by the UV radiation field. The balance between these processes determines the ratio of molecular to atomic hydrogen. In a series of recent papers, Krumholz et al. (2008, 2009) investigate the problem of atomic to molecular ratio with a model that includes the treatment of H$_2$ formation, its self-shielding and the dust shielding. According to their prescription, the molecular fraction in a galaxy is determined primarily by the product of its hydrogen column density and metallicity. Under the assumption of a two-phase medium (Wolfire et al. 1995), the results are largely independent of the UV flux because a change in the UV flux produces a compensating change in the H I density. Hence, the effects of UV radiation field are largely cancelled out. For the purposes of our analysis, the most important prediction of the model by Krumholz et al. is that the fraction of the gas in molecular form increases as the total gas column density $\Sigma_{gas} = \Sigma_{H\,I} + \Sigma_{H_2}$ and the metallicity Z increase, providing a large enough shield against the photodissociation. In agreement with what is observed in local galaxies, the model predicts that the H I column density is expected to saturate at a value of $\sim 10\ M_\odot\ pc^{-2}$. Based on the work by Krumholz et al., it is natural to study the behavior of the total gas column density in our sample to understand the nature of the H$_2$ deficiency.

Figure 5 shows the average total gas surface density profiles $\Sigma_{H\,I} + \Sigma_{H_2}$ in bins of the normalized galactocentric radius. Inside the optical radius, the total gas content of the H I-deficient galaxies (squares) is the same as that of the unperturbed galaxies (circles), while gas-deficient galaxies (triangles) have a lower total gas column density. This behavior reflects the observed atomic and molecular gas content seen in Figure 2, yet add new insights into the nature of the H$_2$ deficiency. Gas-deficient galaxies have a gas column density too low to shield molecules from photodissociation, while H I-deficient galaxies have normal gas content inside their optical radii, which allows the production of molecular hydrogen as in unperturbed galaxies. Indeed, gas-deficient galaxies lie below the critical
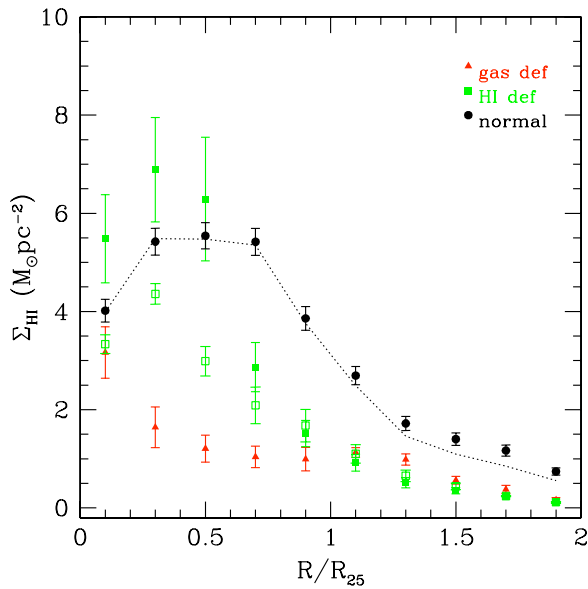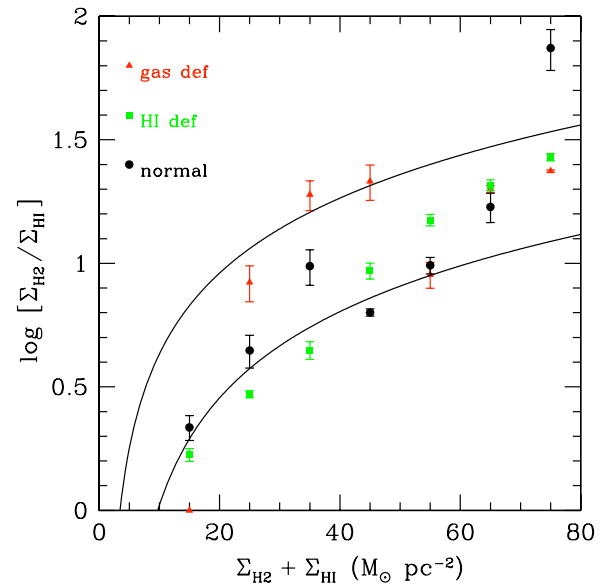
Figure 6. Average H I surface density profiles in bins of normalized radius, divided according to their def$_{HI}$ and def$_{H_2}$ values. The dashed line is computed excluding the H I-rich galaxies with def$_{HI}$ < −0.3 and the open squares indicates the profile for H I-deficient galaxies without NGC 4321. H I-deficient galaxies have in the inner part of the disk an H I column density large enough to form H$_2$.

(A color version of this figure is available in the online journal.)

Figure 7. Ratio of the molecular to atomic hydrogen as a function of the total gas column density. The solid lines show the expected ratio according to the model by Krumholz et al. (2009) for lower ([O/H] = −0.4) and upper ([O/H] = 0) value of metallicity in our sample. At high gas surface densities gas rich and gas poor galaxies exhibit the same behavior because locally the physics of the H$_2$ formation remains unchanged.

(A color version of this figure is available in the online journal.)

shielding column density of $\sim$ 10 $M_\odot$ pc^2 while unperturbed and H I-deficient galaxies lie above this threshold. As in Figure 3, we also plot the average gas profile excluding galaxies with def$_{HI}$ < −0.3 (dashed line): the consistency of the profiles with or without H I-rich galaxies excludes any bias in the mean value toward high column density. Inspecting the individual H I profiles, we noticed that NGC 4321 exhibits an unusual high column density. Excluding this object from the analysis (open squares) does not change the results because the major contribution to the total gas column density comes from the molecular hydrogen.

At this point we have offered an interpretation for why the H I deficiency is only a necessary condition for the in H$_2$ deficiency in H I-poor galaxies, but a new question arises: if unperturbed and H I-deficient galaxies have a comparable gas column density, why do they have different values of def$_{HI}$? The analysis presented in Figure 6 provides the answer. In this plot we show the average H I surface density profiles in bins of the normalized galactocentric radius up to twice R_{25}. As for Figure 5, inspecting the individual H I profiles, we noticed that NGC 4321 exhibits an unusual high column density. To test if this is relevant for our analysis, we overplot with open squares a new H I profile excluding this galaxy. This profile is no longer fully compatible with the one observed for nondeficient galaxies. It is also evident that the surface density profiles for H I-deficient and gas-deficient galaxies exhibit a different behavior. The former rises toward the center, approaching the gas column density observed in unperturbed galaxies, while the latter remains at the lowest observed column density at all the radii. Assuming the profile for unperturbed galaxies serves as a template for how the atomic gas is distributed in spiral galaxies, H I-deficient galaxies have a significant residual quantity of gas toward the center that allows the H$_2$ formation, but have much less H I at larger radii. Therefore, the main contribution to def$_{HI}$ comes from the outer part of the disk where the H I profile rapidly declines. Gas-deficient galaxies have an H I column density that

is reduced relative to that of unperturbed galaxies in both their inner and outer disks and it is only this reduction in the H I content from the inner disk that gives rise to H$_2$ deficiency. The dashed line in Figure 6 shows that the observed behavior is not driven by H I rich galaxies.

In Figure 7 we show the ratio of the molecular to atomic hydrogen as a function of the total gas column density. In this plot, all systematic differences between the classes of galaxy disappear. Since we are exploring the high density regions, the fact that even gas-deficient galaxies show the same behavior observed in nonperturbed and H I-deficient galaxies suggests that molecule formation is a local process within a galaxy and that the relevant local variable is column density. The solid lines in Figure 7 are the expected values of molecular fraction from the model by Krumholz et al. (2009). The model is dependent on the metallicity, so we consider a lower ([O/H] = −0.4) and an upper ([O/H] = 0) value that reasonably correspond to the range of metallicity observed in our sample. There are some approximations that limit the robustness of the comparison between the data and the model. First, the density considered in the model is computed assuming pressure balance, which may not hold in perturbed galaxies; second, we average the gas column density on physical scales that contain several atomic–molecular complexes, while the model is formulated for a single cloud. Despite all these limitations, there is satisfactory agreement between data and the model. Finally, Figure 7 is useful to stress once again the main result of our analysis: galaxies which suffer from H I depletion inside the optical disk are on average shifted at lower column density where the production of H$_2$ becomes inefficient.

4.3. H$_2$ Deficiency and Star Formation

Our analysis offers a possible solution to the current inconsistency in studies of the star formation and galaxy environment. In fact, the observed molecular deficiency is the
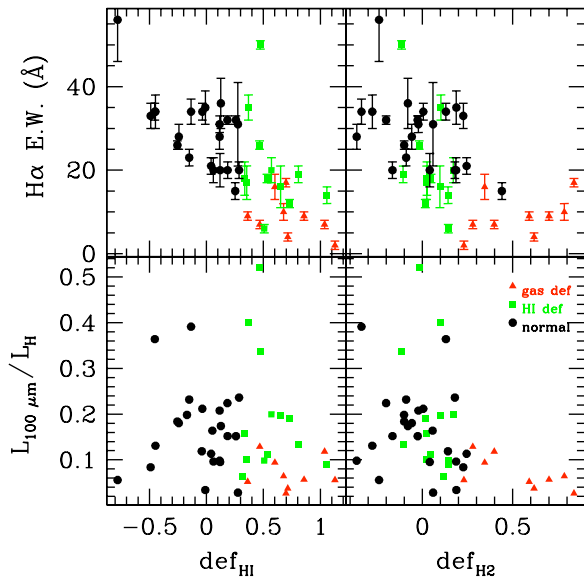
Figure 8. Comparison between the atomic and molecular gas deficiency with SFR indicators. The top panels show the Hα+ [N II] EW, while the bottom panels show the 100 μm luminosity normalized to the *H*-band luminosity. Gas-deficient galaxies have the lowest absolute specific SFR as expected if stars form in molecular rich regions.

(A color version of this figure is available in the online journal.)

missing link between the quenching of the SFR in H I-deficient galaxies (e.g., Gavazzi et al. 2002) and the fact that the bulk of the stars form in molecular regions (Wong & Blitz 2002; Kennicutt et al. 2007; Fumagalli & Gavazzi 2008; Bigiel et al. 2008). Our simple picture is that, when perturbations reduce the atomic hydrogen column density below the threshold required to produce the molecular hydrogen, star formation will be suppressed.

We can test this hypothesis by comparing in Figure 8 the integrated atomic and molecular hydrogen content with our indicator for the star formation activity. The top left panel reproduces the well-known trend (e.g., Gavazzi et al. 2002) between H I deficiency and the quenching of star formation activity, measured through the Hα+ [N II] EW. Gas-deficient galaxies (triangles) clearly exhibit a lower specific SFR than unperturbed (circles) and H I-deficient galaxies (squares). In the top right panel, we plot the Hα+ [N II] EW versus def_{H_2}. Two distinct behaviors can now be identified: molecular hydrogen deficient galaxies (triangles) have their SFR strongly suppressed with respect to molecular rich galaxies (squares and circles). Comparing both the top panels, we conclude that the trend between def_{H_I} and the SFR is in reality a reflection of the link between def_{H_2} and def_{H_I} with def_{H_2} and the SFR. In more detail, looking at the galaxies with $def_{H_I} \geqslant 0.3$ it appears that the H I-deficient galaxies can have SFRs equal to the values observed in nondeficient galaxies, while gas-deficient galaxies have the lowest Hα+ [N II] EW. The dispersion observed in the top left panel can be interpreted as being primarily a product of the observed range in the molecular gas deficiency: not all H I-deficient galaxies are molecular deficient and thus not all them have suppressed star formation. This degeneracy is removed by directly comparing the Hα+ [N II] EW with the def_{H_2}. Because we find the same result by comparing the 100 μm luminosity normalized to the *H*-band luminosity with both def_{H_I} and def_{H_2} (bottom panels), we are confident that dust extinction or [N II] contamination do not significantly affect our conclusions.

5. SUMMARY AND CONCLUSION

Using high-sensitivity and high-resolution CO images from the Nobeyama and the BIMA surveys we have studied molecular hydrogen deficiency in spiral galaxies. Our results and conclusions are summarized as follows.

1. Comparing the total masses of molecular and atomic hydrogen, we detect H_2 deficiency in a subset of galaxies which are H I-poor. The same result is found by studying directly the H_2 surface density profiles. We observe that molecular gas deficiency is associated with the H I reduction inside the optical disk. The deficiency in the atomic hydrogen is a necessary condition for the molecular gas deficiency, but the def_{H_2} parameter spans a wide range of values even in galaxies which are H I-deficient. In fact, there are H I-poor galaxies which have a normal H_2 content.

2. When we examine the molecular fraction at a given point in a galaxy as a function of the total gas column density, we no longer detect any systematic difference between unperturbed, H I-deficient and gas-deficient galaxies. This suggests that the total gas column density, or something strongly correlated with it, is the primary factor in determining the molecular content of a galaxy. In this picture, a galaxy moves from H I-deficient to gas-deficient when it loses enough gas inside its optical disk to bring the gas column density below the critical value of $\sim 10\ M_\odot\ pc^{-2}$ required for H_2 to be present. This behavior is quantitatively consistent with the models of Krumholz et al. (2008, 2009), albeit with significant uncertainties.

3. Since the bulk of the star formation seems connected with the molecular gas, when perturbations reduce the atomic hydrogen column density below the threshold required to produce molecular hydrogen, star formation is suppressed. Studying the Hα+ [N II] EW or the 100 μm luminosity, we show that H_2-deficient galaxies have less star formation than what is observed in H_2–normal galaxies and that the well known trend between the H I deficiency and the SFR most likely reflects a physical connection between molecular hydrogen depletion and star formation activity.

All together, these results corroborate a picture in which the gas phase as a whole feeds the star formation activity. The atomic hydrogen is the essential and primary fuel for the formation of molecular hydrogen that sustains the bulk of star formation activity. When environmental processes or feedback are able to reduce the atomic gas inside the optical disk, the H I column density drops below the critical column density required for molecular hydrogen formation and star formation is quenched. This scenario is supported on cosmological scales, where the H I content in galaxies appears to be unchanged for the past ~ 10 Gyr (Prochaska & Wolfe 2008). This suggests that the global SFR is driven by the accretion of fresh gas from the IGM. In addition, our analysis explains how environmental perturbations or galaxy feedback, which remove the atomic gas, can suppress the formation of the H_2 and stars. The behavior seen in the innermost bin ($0 \leqslant R/R_{25} < 0.2$) of Figures 3, 5, and 6 allows us to rule out the hypothesis that AGN feedback is the dominant process responsible for the gas depletion. In fact, gas is almost unperturbed in the galaxy center. This is expected in our sample where 7/9 of gas-deficient galaxies belong to the Virgo cluster or the Coma 1 cloud in which gas stripping is the most efficient process (Boselli & Gavazzi 2006; Boselli et al. 2006).

Ongoing CO surveys as HERACLES by A. Leroy et al. (2009, in preparation) or JCMT, the Nearby Galaxies Legacy Survey by Wilson et al. (2009), will soon provide larger samples to test our results. A preliminary comparison with the fluxes published by Wilson et al. (2009) appears to support our work. Looking at their Table 4, the four listed galaxies show from the top to the bottom decreasing values of SFR and CO $J : 3–2$ luminosity; consistently, we find for them an increasing value of def_{H_2}. If confirmed, our results support the argument that the bulk of star formation is connected with the molecular gas phase. Moreover, the ability to derive the molecular gas content starting from an observed H I distribution will provide a useful way to correct the SFR expected from local star formation laws (Kennicutt 1998; Bigiel et al. 2008), including the effect of the molecular gas deficiency which suppresses star formation in rich clusters or in interacting galaxies.

Our analysis leaves open a fundamental question on the implications that H_2 deficiency might have for galaxy evolution. In the standard scenario where star formation is supported by cold gas infall toward the inner part of the galaxy halo (Boissier & Prantzos 1999; Dekel & Birnboim 2006), it is fascinating to think that, when the gas flow is halted, the gas is devoured by ongoing star formation. The galaxy depletes its gaseous reservoirs and turns into a passive and quiescent system (van den Bergh 1976). This process might explain a first step for the transition between the blue and red sequence in the color–magnitude diagram. Interactions with the intergalactic medium might thus be an alternative process to AGN feedback or galaxy mergers to explain the departure of star-forming systems from the blue sequence. In our scenario, two timescales govern this migration, one set by the atomic gas depletion and the other related to the response of the star formation activity to the gas removal. The first varies according to the physical process responsible for the H I gas removal, but in this phase the galaxy is still forming stars (e.g., Boselli et al. 2006). The second is a relatively short timescale, at most set by the gas consumption through star formation (~ 2 Gyr, Bigiel et al. 2008),[6] but more likely connected with the much shorter life time of the GMCs. This second phase is consistent with a rapid evolutionary path in the color–magnitude diagram. However, although it has been proved that dwarf galaxies can turn into dwarf ellipticals within ~ 2 Gyr in the local universe (Boselli et al. 2008), it is challenging to prove that massive spirals can turn into giant ellipticals just as a consequence of gas removal through interactions with the cluster IGM. In fact, their angular momentum would be fairly conserved in this kind of interaction. Major mergers as those dominating at higher redshifts must be invoked (Faber et al. 2007).

---

[6] This value comes from the ratio of gas surface density and SFR surface density which is assumed constant. However, gas recycling may increase Σ_{gas} up to 40% and the actual timescale may be longer.
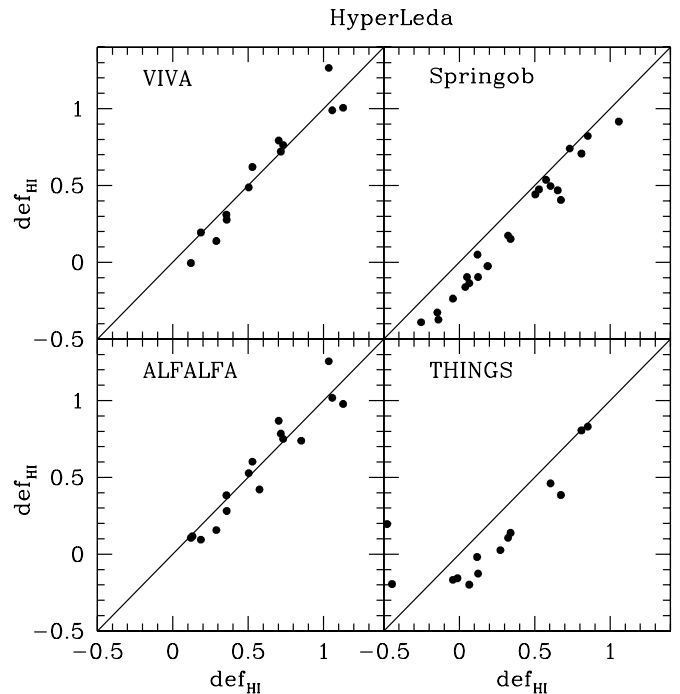
Figure 9. Comparison between the H I deficiency computed using fluxes from HyperLeda (*x*-axis) and from THINGS, VIVA, ALFALFA, and Springob et al. (2005) (*y*-axis). The solid line is the 1:1 correlation.

APPENDIX

H I FLUXES

As discussed in Section 2.2.2, the H I fluxes quoted in the literature for individual galaxies are subject to discrepancies which in some case are not negligible. To show that our result is independent of a particular choice for the H I fluxes, we compute different sets of $def_{H I}$ parameters using fluxes from ALFALFA, THINGS, VIVA, and Springob et al. (2005). Figure 9 shows a comparison of these values with the H I deficiency computed from HyperLeda fluxes adopted in our analysis.

Inspecting the left panels, we notice that $def_{H I}$ computed from ALFALFA and VIVA is in agreement with our values. Because these two surveys provide H I fluxes in the Virgo cluster where the most H I-deficient objects reside, we conclude that $def_{H I}$ for these galaxies is not affected by important fluctuation. In contrast, looking at the right–panels, we notice that at low H I deficiencies a systematic offset appears. Since only few galaxies at low deficiency are available in ALFALFA or VIVA, an additional comparison is almost impossible and it is difficult to further discuss this difference. However, assuming that HyperLeda fluxes suffer from a systematic offset, we should correct our $def_{H I}$ toward even lower $def_{H I}$ values and galaxies

we classify as nondeficient remain in this class. This is not the case for NGC 5236 and NGC 6946, the two outliers visible in the bottom–right panel. However, these galaxies are more extended than the primary beam mapped by THINGS and we are confident that our value for $def_{H I}$ is more accurate.

This comparison confirms that, despite the fluctuation in the $def_{H I}$ parameter, the final distribution for the H I deficiency and thus our analysis are not significantly affected by a particular choice of the H I flux.

REFERENCES

Bigiel, F., Leroy, A., Walter, F., Brinks, E., de Blok, W. J. G., Madore, B., & Thornley, M. D. 2008, AJ, 136, 2846
Boissier, S., & Prantzos, N. 1999, MNRAS, 307, 857
Boselli, A., Boissier, S., Cortese, L., & Gavazzi, G. 2008, ApJ, 674, 742
Boselli, A., Boissier, S., Cortese, L., Gil de Paz, A., Seibert, M., Madore, B. F., Buat, V., & Martin, D. C. 2006, ApJ, 651, 811
Boselli, A., & Gavazzi, G. 2006, PASP, 118, 517
Boselli, A., Gavazzi, G., Donas, J., & Scodeggio, M. 2001, AJ, 121, 753
Boselli, A., Gavazzi, G., Lequeux, J., Buat, V., Casoli, F., Dickey, J., & Donas, J. 1997, A&A, 327, 522
Boselli, A., Lequeux, J., & Gavazzi, G. 2002, A&A, 384, 33
Casoli, F., Boisse, P., Combes, F., & Dupraz, C. 1991, A&A, 249, 359
Decarli, R., Gavazzi, G., Arosio, I., Cortese, L., Boselli, A., Bonfanti, C., & Colpi, M. 2007, MNRAS, 381, 136
Dekel, A., & Birnboim, Y. 2006, MNRAS, 368, 2
Dickman, R. L., Snell, R. L., & Schloerb, F. P. 1986, ApJ, 309, 326
di Serego Alighieri, S., et al. 2007, A&A, 474, 851
Faber, S. M., et al. 2007, ApJ, 665, 265
Fumagalli, M., & Gavazzi, G. 2008, A&A, 490, 571
Gavazzi, G., Boselli, A., Donati, A., Franzetti, P., & Scodeggio, M. 2003, A&A, 400, 451
Gavazzi, G., Boselli, A., Pedotti, P., Gallazzi, A., & Carrasco, L. 2002, A&A, 396, 449
Gavazzi, G., et al. 2008, A&A, 482, 43
Gallazzi, A., et al. 2009, ApJ, 690, 1883
Giovanelli, R., et al. 2005, AJ, 130, 2598
Giovanelli, R., & Haynes, M. P. 1985, ApJ, 292, 404

Haynes, M. P., & Giovanelli, R. 1984, AJ, 89, 758
Helfer, T. T., Thornley, M. D., Regan, M. W., Wong, T., Sheth, K., Vogel, S. N., Blitz, L., & Bock, D. C.-J. 2003, ApJS, 145, 259
James, P. A., et al. 2004, VizieR Online Data Catalog, 341, 40023
Kenney, J. D., & Young, J. S. 1986, ApJ, 301, L13
Kenney, J. D., & Young, J. S. 1988, ApJS, 66, 261
Kenney, J. D. P., & Young, J. S. 1989, ApJ, 344, 171
Kennicutt, R. C., Jr., & Kent, S. M. 1983, AJ, 88, 1094
Kennicutt, R. C., Jr. 1983, ApJ, 272, 54
Kennicutt, R. C., Jr. 1983, AJ, 88, 483
Kennicutt, R. C., Jr. 1992, ApJ, 388, 310
Kennicutt, R. C., Jr. 1998, ApJ, 498, 541
Kennicutt, R. C., Jr., et al. 2007, ApJ, 671, 333
Kennicutt, R. C., Jr., Lee, J. C., Funes, S. J., José, G., Sakai, S., & Akiyama, S. 2008, ApJS, 178, 247
Krumholz, M. R., McKee, C. F., & Tumlinson, J. 2008, ApJ, 689, 865
Krumholz, M. R., McKee, C. F., & Tumlinson, J. 2009, ApJ, 693, 216
Koopmann, R. A., & Kenney, J. D. P. 2004, ApJ, 613, 866
Kuno, N., et al. 2007, PASJ, 59, 117
Meyer, M. J., et al. 2004, MNRAS, 350, 1195
Paturel, G., Petit, C., Prugniel, P., Theureau, G., Rousseau, J., Brouty, M., Dubois, P., & Cambrésy, L. 2003, A&A, 412, 45
Paturel, G., Theureau, G., Bottinelli, L., Gouguenheim, L., Coudreau-Durand, N., Hallet, N., & Petit, C. 2003, A&A, 412, 57
Prochaska, J. X., & Wolfe, A. M. 2008, arXiv:0811.2003
Rengarajan, T. N., & Iyengar, K. V. K. 1992, MNRAS, 259, 559
Solanes, J. M., Giovanelli, R., & Haynes, M. P. 1996, ApJ, 461, 609
Solomon, P. M., Rivolo, A. R., Barrett, J., & Yahil, A. 1987, ApJ, 319, 730
Springob, C. M., Haynes, M. P., Giovanelli, R., & Kent, B. R. 2005, ApJS, 160, 149
Stark, A. A., Knapp, G. R., Bally, J., Wilson, R. W., Penzias, A. A., & Rowe, H. E. 1986, ApJ, 310, 660
Tully, R. B. 1994, VizieR Online Data Catalog, 7145, 0
van den Bergh, S. 1976, ApJ, 206, 883
Vollmer, B., Braine, J., Pappalardo, C., & Hily-Blant, P. 2008, A&A, 491, 455
Wall, W. F. 2007, MNRAS, 379, 674
Walter, F., Brinks, E., de Blok, W. J. G., Bigiel, F., Kennicutt, R. C., Thornley, M. D., & Leroy, A. 2008, AJ, 136, 2563
Wilson, C. D., et al. 2009, ApJ, 693, 1736
Wolfire, M. G., Hollenbach, D., McKee, C. F., Tielens, A. G. G. M., & Bakes, E. L. O. 1995, ApJ, 443, 152
Wong, T., & Blitz, L. 2002, ApJ, 569, 157